View metadata, citation and similar papers at core.ac.uk

brought to you by CORE

provided by DigitalCommons@Fayetteville State University

Fayetteville State University
DigitalCommons@Fayetteville State University

Natural Sciences Faculty Working Papers

College of Arts and Sciences

6-12-2009

Continuum Theory of Carbon Phases

Alexander Umantsev
Fayetteville State University, aumantsev@uncfsu.edu

Zinoviy Akkerman
City University of New York, zakkerman@gmail.com

Recommended Citation

Umantsev, Alexander and Akkerman, Zinoviy, "Continuum Theory of Carbon Phases" (2009). *Natural Sciences Faculty Working Papers*. Paper 14.
http://digitalcommons.uncfsu.edu/natsci_wp/14

This Article is brought to you for free and open access by the College of Arts and Sciences at DigitalCommons@Fayetteville State University. It has been accepted for inclusion in Natural Sciences Faculty Working Papers by an authorized administrator of DigitalCommons@Fayetteville State University. For more information, please contact mlawson@uncfsu.edu.

CARBON 48 (2010) 8–24

available at www.sciencedirect.com

ScienceDirect

journal homepage: www.elsevier.com/locate/carbon

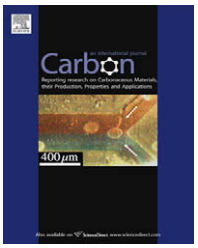

Continuum theory of carbon phases

A. Umantsev[a,*], Z. Akkerman[b]

[a]Department of Natural Sciences, Fayetteville State University, Fayetteville, NC 28301, USA
[b]Department of Physics, City College of the City University of New York, NY 10031, USA

ARTICLE INFO

Article history:
Received 25 February 2009
Accepted 12 June 2009
Available online 21 June 2009

ABSTRACT

We constructed a continuum theory of carbon phases based on the Landau theory of phase transitions. Our theory ties up many seemingly unrelated data on the carbon system. Transformations between graphite, diamond, and liquid-carbon are described by the Landau–Gibbs free-energy which depends on two order parameters: crystallization and structural. The barrier-height and gradient-energy coefficients were calculated from the nucleation data obtained in the studies of diamond/graphite and diamond/liquid-carbon systems. The boundary of the absolute stability of the graphitic phase was interpreted as the spinodal point of the free-energy, which allowed us to calculate the pressure dependence of the barrier-height coefficient. The continuum model yielded a value of 1.66 J/m^2 for the graphite/liquid-carbon interface energy, which continues the trend of the elements of Group IV. We also analyzed stability of nanostructured amorphous carbon and interpreted it as the transition state of the free-energy function. This conjecture helped us to explain results of the experiments on the focused ion-beam irradiation of CVD-diamond nanofilms. The present theory may be used for the large-scale modeling of graphite and diamond crystallization; it can also be extended to include other structural modifications of carbon or an entirely different element such as silicon.

© 2009 Elsevier Ltd. All rights reserved.

1. Introduction

1.1. Carbon phases

Carbon is one of the most abundant elements in the universe and the most versatile material known to a man. This element is the basis of life on Earth and constitutes interiors of the celestial objects: outer planets, Uranus and Neptune, and white dwarf stars. Carbon is often considered to be silicon of the future because of the unique properties resulting from the variety of possible structural forms. A wide range of electronic properties of carbon from insulating/semiconducting diamond to metal-like graphite, nanotubes, and graphene sheets yields many technological applications in different areas of human activity. Such versatility of this element in nature results from the unique property of a carbon atom to form bonds of many different configurations, called hybridizations: liner sp^1, planar sp^2, tetrahedral sp^3, etc. All of this causes great scientific interest in thermodynamic properties of carbon.

Equilibrium carbon phases have been studied for many years. Despite the tremendous technical difficulties of experimental studies (temperatures of up to 10,000 K and pressures of 100–1000 GPa) the phase diagram of carbon has been created [1–3]. Thermodynamic databases helped develop fairly good bulk-thermodynamic free-energy functions that reproduce the low-temperature portion of the carbon phase diagram [4]. Because of the experimental difficulties, the theoretical (density functional) and numerical (MC and MD) methods of study of carbon phases gained popularity in the scientific community [5–15]. The phase diagram of carbon most commonly considers three clearly distinguished phases:

* *Corresponding author:* Fax: +1 910 6721159.
E-mail address: aumantsev@uncfsu.edu (A. Umantsev).
0008-6223/$ - see front matter © 2009 Elsevier Ltd. All rights reserved.
doi:10.1016/j.carbon.2009.06.032

graphite, diamond, and liquid carbon, although there is a number of high energy phases, e.g. bc8 and simple cubic, which were found to be metastable at low pressure and temperature [5] and stable at high pressure conditions [6]. Analysis of the behavior of graphite under conditions of isotropic pressure brought a surprising result that at least its rhombohedral modification can transform into diamond without thermal activation at 80 GPa [7]. Although these studies are still work in progress and the experimental phase diagram in its finality is still to be drawn, many features have been clarified recently: for instance, a triple point of coexistence of the three phases has been found to be around the temperature of 4250 K and pressure of 15 GPa, see [8] and Fig. 1.

Experimental results on liquid carbon are scarce because of the extreme conditions and/or short times of observations of the liquid state. However, a maximum in the melting temperature of graphite as a function of pressure has been observed in a number of studies [1–3]. Explanations of the maximum led to the introduction of two types of liquids: low-pressure graphite-like predominantly-sp^2 and high-pressure diamond-like predominantly-sp^3 [15]. Ree et al. [9–11] conducted MD simulations and presented the isotherms of liquid carbon exhibiting a clear Van der Waals type dependence between the mostly sp^2 and sp^3 liquids. As a result, a liquid–liquid phase transition (LLPT) has been predicted. Moreover, a second triple point of coexistence of the two liquids and graphite and a critical point of the coexistence of the two liquids at the temperature around 9000 K and pressure of 11 GPa have been conjectured [9–11], although these did not follow from the experimentally observed properties of the liquid [1–3]. Numerical modeling of carbon structures relies heavily on the choice of the interaction potential, which is being constantly revised approaching the "real" interaction of carbon atoms. Recently Wang et al. [12] and Ghiringhelli et al. [8] presented calculations using an improved interaction potential and found no evidence of LLPT or the critical point for liquid carbon. However, there are no doubts that as pressure increases atomic coordination of carbon undergoes an adjustment from three- to four- and higher-fold numbers [6].

Carbon may also exist in another solid-state form, amorphous [16,17]. Classification of carbonacious materials as 'amorphous' is not straightforward as many different systems fall into this category. One of the important parameters of such materials is the sp^3/sp^2 ratio. Amorphous carbon with high ratio, usually at or above 70%, is called tetrahedral (ta-C); it is also often called diamond-like carbon due to similarity of electrical and mechanical properties of ta-C to those of diamond. There is another category of amorphous carbon that attracts attention of the researchers-*nanostructured amorphous carbon* (na-C). Na-C can be manufactured using several different techniques: chemical vapor deposition (CVD) of carbon atoms, focused ion beam bombardment (FIB) of carbon

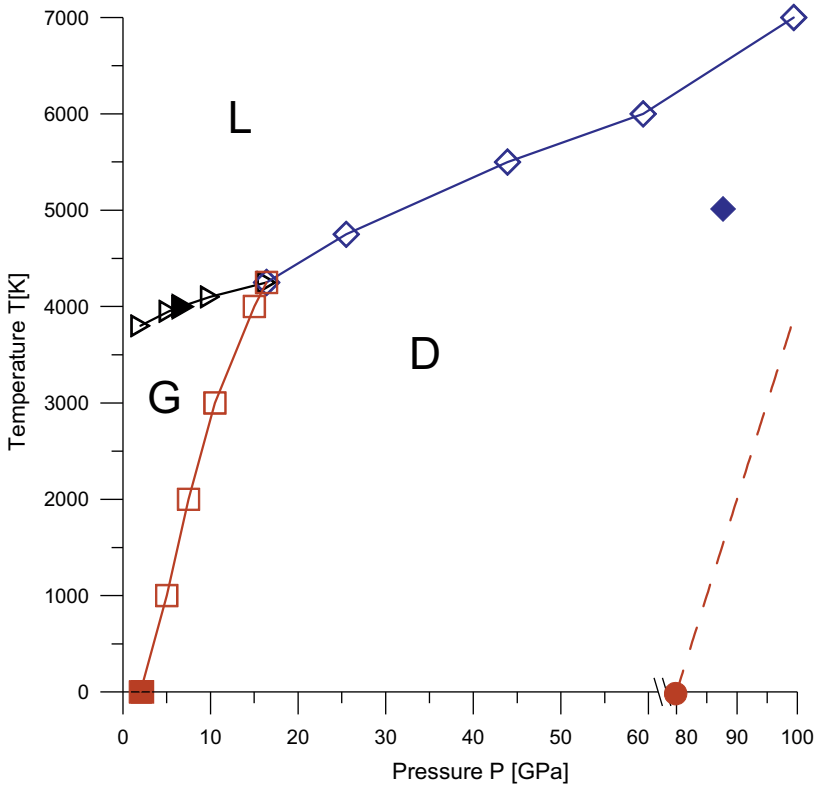

Fig. 1 – Low temperature–pressure region of the carbon phase diagram. G-graphite, D-diamond, L-liquid carbon regions. Solid lines-phase boundaries based on the data of [8]; dashed line-graphite/diamond spinodal line based on the data of [7]. Red square-($T = 0$ K, $P = 1.36$ GPa); red circle-($T = 0$ K, $P = 80$ GPa); black triangle-($T = 4000$ K, $P = 6.7$ GPa); blue diamond-($T = 5000$ K, $P = 85$ GPa). (For interpretation of the references to color in this figure legend, the reader is referred to the web version of this article.)

surfaces with non-carbon ions [18–20], etc. Regardless of the preparation technique na-C's have two common features. First, these materials are always produced in the form of thin films, wires, or small particles that is, nanostructures. Second, although theoretical calculations and numerical simulations of such materials produced energies of formation significantly higher than those of graphite and diamond at the same temperatures [13,21–23], these materials possess certain degree of thermodynamic stability.

The MD/MC cluster simulation methods are an excellent tool of materials study when equilibrium properties of phases-graphite, diamond, liquid, and amorphous-are considered [5–13]. These methods, however, encounter significant difficulties describing nucleation of the new phases [24] because they deal with relatively small clusters of atoms and do not allow for the analysis of heterosystems. As a result, stability of na-C can hardly be analyzed based on the cluster simulation methods. Another important area where these methods fail is the kinetics of phase transformations. A different method, which would allow for the analysis of the interface regions and kinetics, is required for the uninterrupted progress of the study of carbon.

1.2. *Continuum method of phase transitions*

A *continuum approach* can serve this purpose. Many researchers have noticed that there are continuous transformation paths between different phases of carbon [5,7]. In this publication we discuss our efforts to build a Landau-type theory of carbon phases [25,26]. The theory does not introduce a new phase diagram of carbon but uses already existing data on phase boundaries of the diamond, graphite, and liquid phases [1–14]. Specifically, we will be using the database of [4] for the low-temperature region $(0-3000\,\mathrm{K})$ and the thermodynamic calculations of [8] for the high-temperature region $(3000-6000\,\mathrm{K})$ of the phase diagram. The theory has proven to be able to analyze a variety of systems [27,28]; it provides a universal approach to a variety of processes and has an important advantage of analyzing both stability and transformation kinetics incorporating the thermodynamic and dynamic data into a unified scheme. To the best of our knowledge this is the first application of the theory to a system with pure covalent bonding. Most of the results of the paper relate to the region of the diagram near the graphite/diamond/liquid triple point, Fig. 1.

The Landau theory of phase transitions is a mean-field type of theory. In the framework of this theory a state of a system, in addition to the thermodynamic variables like temperature T and pressure P, is represented by a certain value of a 'hidden' variable η, called an *order parameter* (OP) [25,26]. OP is a low-dimensional characteristic of a particular transformation in a multi-dimensional space. The transformation is fully characterized by the *coarse-grained* free energy, which may be significantly simplified by taking into account all the symmetries of the system. Introduction of the OP allows one to define a *phase* as a locally stable homogeneous (with respect to the OP) state of the system. As known, in an open one-component system, a phase corresponds to a minimum of the molar Gibbs free energy, $G(T,P,\eta)$. Hence, the OP for this state can be found among the critical points of G as a function of OP:

$$\left(\frac{\partial G}{\partial \eta}\right)_{T,P}=0 \tag{1}$$

The free energy function that describes a phase transition must have at least two minima with respect to OP that correspond to the phases: $\eta=\eta_0$, and $\eta=\eta_1$ (e.g. $\eta_1>\eta_0$), and a maximum, which corresponds to the *transition state*, $\eta=\eta_t$, that is, the barrier that separates the basins of stability of the phases. Transition state, a free-energy maximum with respect to OP, can also be found among the roots of Eq. (1) but, contrary to the bulk phases, it is locally unstable under the conditions of constant pressure that is $(\partial^2 G/\partial\eta^2)_{T,P}(\eta_t)<0$, see Inset (a) of Fig. 2. The phase-equilibrium temperature or pressure P_E, is defined by the equation $G(T,P_E,\eta_0)=G(T,P_E,\eta_1)$. A system may also have one or several *spinodal points* that is, temperature and pressure values (T,P_S) where a metastable phase ultimately loses its stability and becomes absolutely unstable (see Figs. 1 and 2). Experimentally the spinodal points manifest themselves in disappearance of a need for thermal or chemical activation for the transition. In the language of the continuum theory the spinodal points appear when the OP of the transition state becomes equal to that of the metastable phase, e.g.

$$\eta_t(T,P_S^0)=\eta_0(T,P_S^0) \tag{2}$$

Many systems cannot be described by a single OP due to variety of transitions that may occur simultaneously. In this case the most convenient way to define the order parameters is to set them as independent. Even with two independent OP the free energy $G(T,P,\eta,\xi)$ has significantly greater variety of types of the critical points than with one, the most popular additional type is the saddle point [29]. The sufficient condition of local minimum at the two-OP critical point is that:

$$\frac{\partial^2 G}{\partial \xi^2}>0,\quad \text{and}\quad \frac{\partial^2 G}{\partial \eta^2}\frac{\partial^2 G}{\partial \xi^2}-\left(\frac{\partial^2 G}{\partial \eta\partial \xi}\right)^2>0 \tag{3}$$

In the framework of the continuum field-theoretic approach of the Landau theory the structural *heterogeneities* are described by the gradients of the OP so that the molar Gibbs free energy of the substance is expressed as follows [30–32]:

$$\widehat{G}=G(T,P,\eta)+\frac{1}{2}\kappa(T,P)(\nabla\eta)^2 \tag{4}$$

where κ is called the *gradient-energy* coefficient. Thus, the *total* Gibbs free energy of the system of volume V is

$$\mathcal{G}\{T,P,\mathcal{N},\eta(\mathbf{r})\}\equiv\int_V \rho\widehat{G}d^3x \tag{5}$$

where ρ is the molar density (V is the molar volume):

$$\rho^{-1}\equiv\left(\frac{\partial G}{\partial P}\right)_{T,\eta}=V \tag{6}$$

and $\mathcal{N}$ is the number of moles in the system:

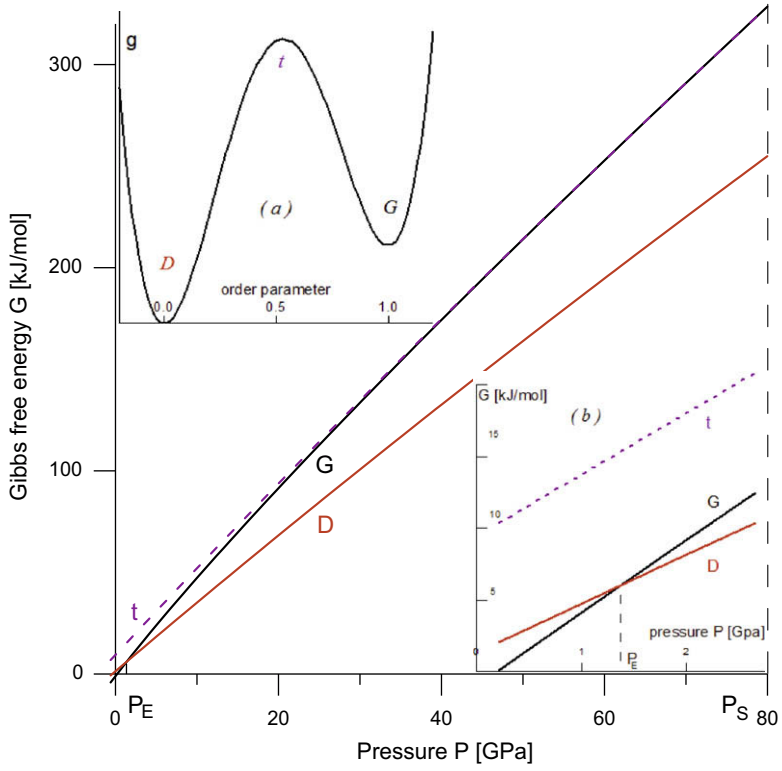

Fig. 2 – Gibbs free energy G of the diamond (D) and graphite (G) phases and the transition state (t) as functions of pressure P at $T = 0$ K using the database of [4] and estimates of Eq. (29). Inset (a) Normalized Gibbs free energy g as a function of the order parameter at $P > P_E$. Inset (b) G's as functions of P near the equilibrium value $P_E = 1.36$ GPa.

$$\mathcal{N} \equiv \int_{\mathcal{V}} \rho d^3x = \text{const}(T, P) \tag{7}$$

Taking into account the constraint of fixed number of moles $\mathcal{N}$ in the system[1] we obtain that the open-system variational problem $(G \to \min, \mathcal{N} = \text{const}, \mathcal{V} \neq \text{const})$ yields the following boundary-value problem [33] for the equilibrium distribution $\eta_E(\mathbf{r})$:

$$\frac{\partial \rho(G-\mu)}{\partial \eta} - \nabla\left(\rho \frac{\partial \widehat{G}}{\partial \nabla \eta}\right) = 0 \quad \text{in } \mathcal{V}; \tag{8a}$$

$$\mathbf{n} \cdot \nabla \eta = 0 \quad \text{on } \widehat{\mathcal{V}}; \tag{8b}$$

$$\rho[G - \mu - \kappa/2(\nabla\eta)^2] = 0 \quad \text{on } \widehat{\mathcal{V}}; \tag{8c}$$

Here μ is the chemical potential of the system which depends on T, P, and V; $\widehat{\mathcal{V}}$ is the boundary of V, and $\mathbf{n}$ is the unit vector on $\widehat{\mathcal{V}}$. The free-boundary condition, Eq. (8c), appears because the volume of an open system is not specified. From the boundary conditions, Eqs. (8b) and (8c), follows that

$$\mu = G(T, P_E, \eta_E\{\widehat{\mathcal{V}}\}). \tag{9}$$

Coexistence of two phases at equilibrium entails a layer between them called an *interface*. Many properties of an interface at equilibrium in a one-component medium can be completely determined by just one intensive quantity, the surface tension or *interface free energy* σ [34]. In the continuum formulation the interface is represented by a transition zone of certain thickness l where the OP changes its value from that in the bulk of one phase, e.g. η_0, to that in the bulk of the other one, e.g. η_1. Then the interfacial energy and thickness can be defined as follows [32]:

$$\sigma \equiv \int_{-\infty}^{+\infty} \rho[\widehat{G}(T, P_E, \eta_E) - \mu]dx; \quad l \equiv \frac{|\eta_1 - \eta_0|}{\max|d\eta/dx|}. \tag{10}$$

In the case of a one-dimensional system with the size X in the direction perpendicular to the plane of the interface, the Euler equation, Eq. (8a), can be integrated once. Taking into account the free-boundary condition, Eq. (8c) and the fact that $\rho \neq 0$, we find that the 1D open-system equilibrium-state boundary-value problem takes the form:

$$G(T, P_E, \eta_E) - \frac{\kappa}{2}\left(\frac{d\eta_E}{dx}\right)^2 = \mu \quad \text{for} \quad 0 < x < X, \tag{11a}$$

$$\frac{d\eta_E}{dx} = 0 \quad \text{for} \quad x = 0, X. \tag{11b}$$

Then one can find the expressions for σ and l in an unlimited $(X \to \infty)$ open system:

$$\sigma = \sqrt{2\kappa}\int_{\eta_0}^{\eta_1} \frac{\rho d\eta}{\sqrt{G_E - \mu}}; \quad l = |\eta_1 - \eta_0|\sqrt{\frac{\kappa/2}{G_E - \mu}} \tag{12}$$

In the case of two OP's:

$$\widehat{G} = G(T, P, \eta, \xi) + \frac{1}{2}\kappa_\eta(T, P)(\nabla\eta)^2 + \frac{1}{2}\kappa_\xi(T, P)(\nabla\xi)^2 \tag{13}$$

[1] We define $q \equiv \text{const}(u)$ as a quantity that does not depend on u but may depend on other variables of the problem.

If the molar density does not vary strongly, it may be assumed a constant, $\rho = \bar{\rho} = \text{const}(x)$, and the interface energy may be expressed as follows [35]:

$$\sigma = 2\bar{\rho}\int_{-\infty}^{+\infty}\{G(T,P_E,\eta_E,\xi_E)-\mu\}dx = \bar{\rho}\int_{-\infty}^{+\infty}\left\{\kappa_\eta\left(\frac{d\eta_E}{dx}\right)^2+\kappa_\xi\left(\frac{d\xi_E}{dx}\right)^2\right\}dx \quad (14)$$

1.3. Stability of transition state in closed systems

The transition state of the single-OP homogeneous system, η_t, corresponds to a maximum of $G(T,P,\eta)$ with respect to the OP variations and is absolutely unstable (that is, with respect to small fluctuations of η) in an open system (that is, for $T,P = \text{const}$). However, the stability of this state can change dramatically in a *closed system* when the condition of constant volume is imposed: $V = \text{const}$. In this case instead of the molar Gibbs free energy as a function of pressure, $G(T,P,\eta)$, it is more convenient to use the molar Helmholtz free energy, $F(T,V,\eta)$, as a function of the molar volume V, Eq. (6). The latter can be found from the former through the Legendre transformation:

$$F(T,V,\eta) = G - P\left(\frac{\partial G}{\partial P}\right)_{T,\eta}$$

Recently one of the authors (AU) used the continuum method to analyze the case of a closed system and showed [36] that a homogeneous transition state, η_t, can be thermodynamically stable if:

$$\left.\frac{\left(\frac{\partial^2 G}{\partial P\partial\eta}\right)^2}{\frac{\partial^2 G}{\partial\eta^2}\frac{\partial^2 G}{\partial P^2}}\right|_{\eta=\eta_t} > 1. \quad (15)$$

As known, in a closed system of given size and average molar volume a heterogeneous mixture of the bulk phases is more stable than any other homogeneous state of the system. However, as it was demonstrated in [36], if the size of the closed system X is below the critical limit X_{cr}:

$$X < X_{cr} \equiv \frac{\pi}{2\sqrt{2}}l, \quad (16)$$

the homogeneous transition state can be globally stable that is, have less Helmholtz free energy than any other equilibrium state including heterogeneous ones. Thus, if the material parameters of the system satisfy the criterion, Eq. (15), and the linear sizes – (16) then the homogeneous transition state, η_t, becomes the most stable state of the closed system in the certain range of average molar volumes.

The structure of the paper is as follows. In Section 2 we introduce a continuum model of carbon phases and demonstrate how the parameters of the model may be obtained from the data on nucleation of diamond on graphite and from liquid. In Section 3 we apply the developed model to the problem of crystallization of graphite by considering the processes of nucleation of graphite from liquid phase. The model will be also used in the present paper to gain an insight into the equilibrium properties of the amorphous phase of carbon at nanoscale dimensions (na-C) and amorphization of carbon under conditions of FIB irradiation of CVD-diamond nanofilms [18–20]. In Section 4 we discuss the obtained results and extensions of the model on different systems.

2. Continuum model of carbon

2.1. Order parameters

The choice of OP's for a real-material continuum modeling is always a complicated matter. As we pointed out in the Introduction our goal is to construct a model that describes the processes of carbon melting-crystallization and the graphite–diamond structural transformation. To describe the variety of possible structural forms and different transformations of carbon in the region of the phase diagram near the graphite/diamond/liquid triple point, see Fig. 1, we need at least two OP's, which may be multi-component and depend on three spatial coordinates. To describe crystallization we use the approach of Ramakrishnan and Yussouff [37] where the authors proved that"the lattice periodic component of the density is... an order parameter" for freezing transition. In the Landau–Gibbs free energy proposed below the *effective scalar crystallization* OP η that distinguishes a solid state from a liquid one may be interpreted as the crystal-lattice Fourier component of the density.

Dmitriev et al. [38,39] interpret "the graphite–diamond transition ... as a transition between two low-symmetry ordered phases, which are derived from a common disordered hexagonal latent parent phase". It was also found in [38,39] that "an essential parameter appears to be the degree of occupancy of the latent unit cell by the atoms (i.e., the concentration)." The treatment in [38,39], however, did not produce a phase diagram of carbon as a real material, which should be accomplished by our model. That is why we will be using an *effective scalar structural* OP ξ associated with the graphite–diamond transition, which describes the most favorable path between the graphite and diamond phases in the multi-dimensional space of the structural OP's.

Diversity of atomic configurations of solid carbon is usually characterized by the *average coordination number* C, which is defined as the number of other atoms directly linked to the specified atom. In the literature [13,23] one may find a working definition of the average coordination as the number of neighbors in a sphere of certain radius, usually about 1.85 Å. On the microscopic scale the average coordination number relates to the state of atomic hybridization: sp^3, sp^2 or sp^1. On the macroscopic scale C is connected to the properties of the material; e.g. the molar density ρ of carbon structures [16,17,23]. As the definition of C relates to the coarse-grained nature of the effective OP's, their physical meaning may be clarified through the relationship with $\rho : C = \Phi\{\rho(T,P;\eta,\xi)\}$, where the density of the system in the entire domain of variation of temperatures and pressures can be found using Eq. (6).

A reliable relationship $C = \Phi\{\rho\}$ for different structural modifications of carbon should be a subject of an independent study. In this paper we use a linear approximation of this relationship; such approximation was found to be approximately correct in amorphous carbon [16,17,23]. As the function $C = \Phi\{\rho\}$ must pass through the densities of graphite

$(\rho = \rho_G, C = 3)$ and diamond $(\rho = \rho_D, C = 4)$, it can be expressed as follows:

$$C(T,P,\eta,\xi) = 3 + \frac{\rho(T,P,\eta,\xi) - \rho_G(T,P)}{\rho_D(T,P) - \rho_G(T,P)} \tag{17}$$

This relationship spreads beyond the values of graphite and diamond phases into the domains of densities typical for the liquid carbon and high-energy phases.

2.2. Gibbs free energy of carbon

Although the energies of formation of different carbon structures are very close, they must be separated by high activation barriers, which provide their stability in a wide range of conditions. For instance, diamond is stable at room temperature and pressure although it is thermodynamically unstable against graphite phase under these conditions. Both transitions, structural and crystallization, are of the first-order; hence, the free-energy function of carbon must be a polynomial of the order not less than fourth and include the terms of the third order in ξ and η. The OP's coupling must start with the bi-quadratic term and have the form that excludes the stability of the phases other than diamond, graphite, and liquid. On the basis of these facts we propose the following form of the Landau–Gibbs free energy:

$$G(T,P;\eta,\xi) = Q + \frac{1}{2}A_\eta\omega^2(\eta) + B_\eta v(\eta) + \frac{1}{2}A_\xi\omega^2(\xi) + B_\xi v(\xi) + Jv(\xi)v(1-\eta) \tag{18a}$$

where A's, B's, Q, and J are functions of (T,P), which should be determined through the comparison with the phase diagram of carbon. The OP's can always be scaled such that their values at the stable phases are near 0 and 1; this constraint allows us to select the functions $\omega(x)$ and $v(x)$ as

$$\omega(x) = x(1-x); \quad v(x) = x^2(3-2x) \tag{18b}$$

The equilibrium phases-graphite, diamond, and liquid – can be found among the critical points (ξ_C, η_C) of the free energy G, Eq. (18), that is, the solutions of the following simultaneous equations:

$$\begin{aligned} \frac{\partial G}{\partial \xi} &= \omega(\xi)[A_\xi\omega'(\xi) + 6B_\xi + 6Jv(1-\eta)] = 0 \\ \frac{\partial G}{\partial \eta} &= \omega(\eta)\left[A_\eta\omega'(\eta) + 6B_\eta - 6Jv(\xi)\right] = 0 \end{aligned} \tag{19}$$

Eq. (19) can be easily resolved and the critical points (ξ_C, η_C) can be found as the intersections of the pairs of the critical lines from the following two sets:

$$\xi_0 = 0; \quad \xi_t = \frac{1}{2} + \frac{3}{A_\xi}[B_\xi + Jv(1-\eta)]; \quad \xi_1 = 1 \tag{20a}$$

$$\eta_0 = 0; \quad \eta_t = \frac{1}{2} + \frac{3}{A_\eta}[B_\eta - Jv(\xi)]; \quad \eta_1 = 1 \tag{20b}$$

According to the definition presented above, a phase is a locally stable homogeneous state of a system. Hence, to identify the OP's of the phases we have to verify Eq. (3) for the critical points (ξ_C, η_C). As the second-order partials of G are:

$$\begin{aligned} \frac{\partial^2 G}{\partial \xi^2} &= A_\xi\{\omega(\xi)\omega''(\xi) + [\omega'(\xi)]^2\} + 6\omega'(\xi)[B_\xi + Jv(1-\eta)] \\ \frac{\partial^2 G}{\partial \eta^2} &= A_\eta\{\omega(\eta)\omega''(\eta) + [\omega'(\eta)]^2\} + 6\omega'(\eta)[B_\eta - Jv(\xi)] \\ \frac{\partial^2 G}{\partial \eta \partial \xi} &= -36J\omega(\xi)\omega(\eta) \end{aligned} \tag{21}$$

the condition, Eq. (3), will be satisfied if we choose the phases as following: liquid $= (\xi_0, \eta_0)$; diamond $= (\xi_0, \eta_1)$; graphite $= (\xi_1, \eta_1)$. Such choice of phases helps identify parameters Q, B_ξ, and B_η of the free energy, Eq. (18), as following:

$$\begin{aligned} Q &= G_L(T,P) \\ B_\eta &= G_D(T,P) - G_L(T,P) \equiv \Delta G_{D/L} \\ B_\xi &= G_G(T,P) - G_D(T,P) \equiv \Delta G_{G/D} \end{aligned} \tag{22}$$

where $\Delta G_{D/L}$, $\Delta G_{G/D}$ may be called the *driving forces* of the respective transitions.

The free energy, Eqs. (18) and (22), has another critical point – (ξ_1, η_0) with liquid-like OP η. As pointed out in the Introduction there is no LLPT in the carbon system. To exclude the second liquid phase from our system we assume that this state represents a saddle point of the free energy:

$$\eta_t(\xi = \xi_1) = \eta_0. \tag{23}$$

This yields a constraint on the interaction parameter J:

$$J = \frac{1}{6}A_\eta + \Delta G_{D/L} \tag{24}$$

Thus the molar Gibbs free energy of carbon takes the form:

$$\begin{aligned} G(T,P;\eta,\xi) = G_L &+ \frac{1}{2}A_\eta\omega^2(\eta) + \Delta G_{D/L}v(\eta) + \frac{1}{2}A_\xi\omega^2(\xi) \\ &+ \Delta G_{G/D}v(\xi) + \left(\frac{1}{6}A_\eta + \Delta G_{D/L}\right)v(\xi)v(1-\eta) \end{aligned} \tag{25}$$

where A_η, A_ξ are called the *barrier-height coefficients* because at equilibrium the phases are separated by the free energy barrier of the height $A/32$. Notice that redefinition of the OP's does not change the heights of the free energy barriers.

Fig. 3 represents a phase map – the critical lines in the plane (ξ, η) – of the Landau–Gibbs free energy, Eq. (25), with the values of $G_{L(G,D)}(T,P)$ obtained from [8] and parameters, A_η, A_ξ identified in the following sections. The stable (and metastable) phases satisfy the conditions of Eqs. (3) and (21) and the saddle points represent the transition states between the phases. In Fig. 4 is depicted the stereoscopic projection of the Landau–Gibbs free energy, Eq. (25), as a function of OP's (ξ, η) at the same point in the (P,T)-phase diagram of Fig. 1 as in Fig. 3 that is, on the graphite melting line.

The free energy density of the continuum theory, Eqs. (13) and (25), contains a set of coefficients, the barrier-height A's and the gradient-energy κ's. For instance, inclusion of the gradient energy contributions into the theory accounts for the heterogeneities of the material, which in the case of carbon are due to the stretching and bending of atomic bonds that is, stresses in the system. As these coefficients are not standard, tabulated properties of materials one needs to find means of estimating them. For the consistency of the continuum theory it is preferable to estimate them *directly* from the *ab initio* calculations. Because this problem is not solved yet, in the following two sections the coefficients (A_η, κ_η) and (A_ξ, κ_ξ) will be identified *indirectly* via the comparison with the appropriate quantities obtained from the results of the simulations of nucleation of diamond phase from graphite and liquid carbon. We will also estimate the (T, P)-dependence of these coefficients using the data on stability of carbon phases.

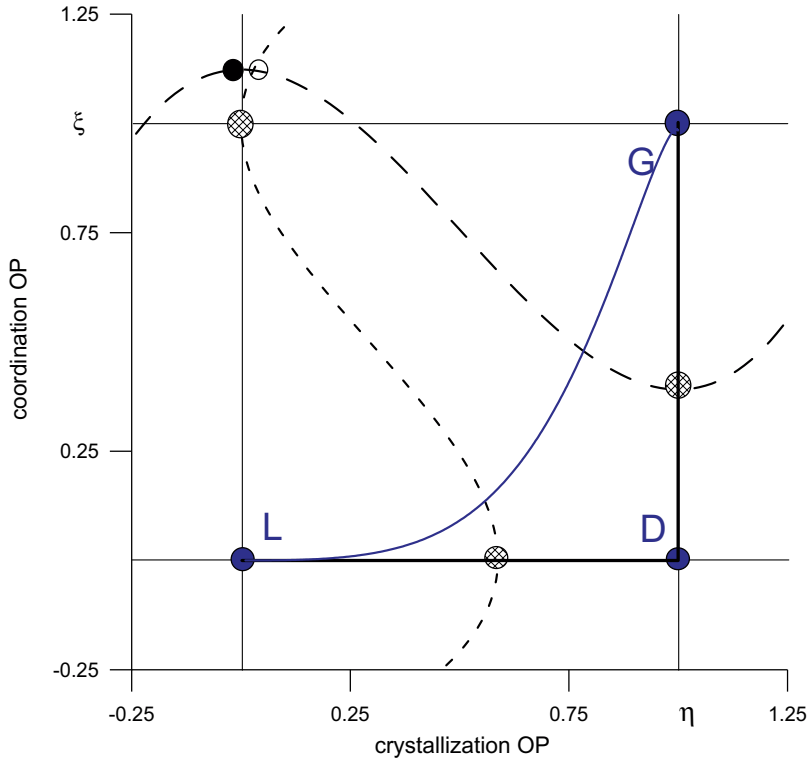

Fig. 3 – Phase map-plane of the structural and crystallization OP's-for the 'black triangle' point ($T = 4000$ K, $P = 6.7$ GPa) on the graphite melting line in Fig. 1. Black lines are the critical lines, Eq. (20); solid lines: $\xi = \xi_{0.1}$ and $\eta = \eta_{0.1}$; dashed lines: $\xi = \xi_t(\eta)$ and $\eta = \eta_t(\xi)$. Circles are the critical points (ξ_c, η_c): full blue circles-stable phases, full black circle-metastable state, crosshatched circles-saddle points, open circle-local maximum of the free energy. Thick lines-trajectories that represent the interfaces: black-diamond/graphite and diamond/liquid-carbon, blue-graphite/liquid-carbon. (For interpretation of the references to color in this figure legend, the reader is referred to the web version of this article.)

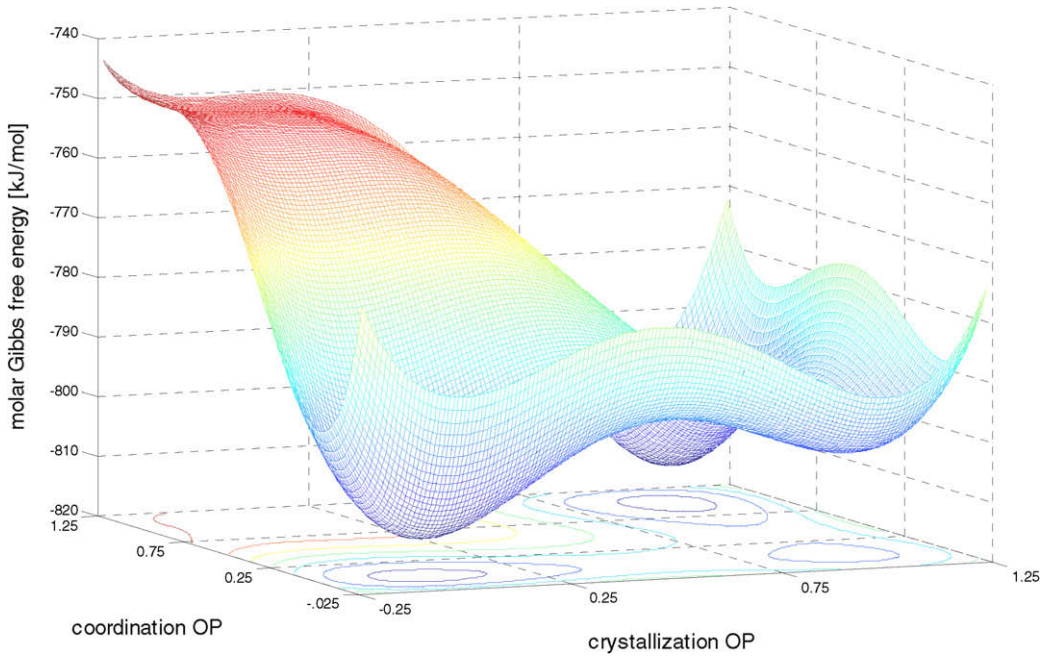

Fig. 4 – Stereoscopic projection of the Landau–Gibbs free energy, Eq. (25), for the conditions of Fig. 3.

2.3. *Diamond/graphite coexistence*

As known, the interfacial energy plays a major role in the processes of nucleation and epitaxial growth of one phase on the surface of another, e.g. diamond on graphite [16]. To calculate the excess of the total energy of a non-hydrogenated graphite/diamond interface Lambrecht et al. [40] used the method of continuous matching of diamond and graphite planes for two possible structures: (i) two $(1\bar{1}00)$ graphite planes matching three $(1\bar{2}1)$ diamond planes and (ii) two $(11\bar{2}0)$ graphite planes matching three $(10\bar{1})$ diamond planes. The coherency of the graphite/diamond interface will be warranted in both cases if three {111} diamond planes match up with two {0001} graphite planes. The model yielded quantitative structures of the interfaces at 0 K where the excess energy was "essentially due to (the presence of) the dangling bonds". For the magnitudes of $\sigma_{D/G}$ the authors found: (i) 1.7 J/m^2 and (ii) 2.5 J/m^2; they argued that this result explained the fact that type-(i) interface is the most frequently observed in the experiments.

The interfacial structure presented in [40] allowed us to estimate the thickness of the interface $l_{D/G}$. In addition to sp^2-sp^2 and sp^3-sp^3 bonds, the interface includes sp^2-sp^3 and dangling bonds. As it can be expected, the graphite planes are affected greater by the coherent matching than those of the diamond phase. We estimate that two layers of the graphite, two layers of the transition zone, and one layer of the diamond phase are affected by the transition. Then, taking into account angular orientation of the diamond bonds and using the value of 1.42 Å for the average bond length, the total thickness of the type-(i) interface $l_{D/G}$ comes to about 0.57 nm. Although this result was obtained from the analysis of one orientation only, it provides a good starting point for numerical analyses of the model.

In the continuum theory a phase-separating interface is described by the interfacial energy σ and thickness l from Eq. (10). In the present subsection we consider the solid-state transformation of carbon between the diamond and graphite phases. As the terminal phases of the transformation path defined by the free energy, Eq. (25), have the same crystallization OP $\eta=\eta_1$, the entire diamond/graphite interface may be described by Eq. (12) with only one, structural OP ξ, varying (the thick black vertical line in Fig. 3). Then we obtain (see details in [36]):

$$\sigma_{D/G}=\frac{1}{6}\sqrt{\kappa_\xi A_\xi}\,\frac{\ln V_G/V_D}{V_G-V_D},\quad l_{D/G}=4\sqrt{\frac{\kappa_\xi}{A_\xi}} \tag{26}$$

Given the estimates of $l_{D/G}$ and $\sigma_{D/G}$ for the type-(i) graphite/diamond interface and the magnitudes of $V_G=5.082$ cc/mol, $V_D=3.406$ cc/mol, we estimate the magnitudes of the barrier-height A_ξ and gradient-energy κ_ξ coefficients at $(T=0\,\mathrm{K},\ P_E=1.36\,\mathrm{GPa})$ as follows:

$$\begin{aligned} A_\xi &= 24\frac{\sigma_{D/G}}{l_{D/G}}\frac{V_G-V_D}{\ln V_G/V_D}\approx 300.\frac{kJ}{mol};\\ \kappa_\xi &= \frac{3}{2}\sigma_{D/G}l_{D/G}\frac{(V_G-V_D)}{\ln V_G/V_D}\approx 0.609\times 10^{-15}\frac{Jm^2}{mol}. \end{aligned} \tag{27}$$

The activation barrier height at equilibrium, $A_\xi/32\approx 9.4$ kJ/mol (~ 0.1 eV/atom) can be compared with the driving force for the diamond-to-graphite transition at (0 K, 0 GPa), which, using the data of [4], can be estimated as 2.7 kJ/mol, and the thermal energy at (300 K, 0 GPa) of 2.5 kJ/mol. We can conclude that the activation barrier significantly impedes transition of diamond to the more stable graphite phase as the experiment shows. In Fig. 2 are depicted the Gibbs free energies of graphite and diamond phases and the transition state versus pressure at 0 K. As the results of [40] are applicable only to the specific direction of matching diamond and graphite planes, the magnitudes of A_ξ and κ_ξ should be orientation sensitive.

Fahy et al. [7], using the density-functional theory with an *ab initio* pseudopotential and the interlayer distance as a free parameter, calculated the activation barrier between rhombohedral graphite and diamond to be 0.33 eV/atom. This estimate, which seems to eliminate practically any thermally activated diamond–graphite transition at temperature below 2000 K, is significantly greater than ours not only because they considered a rhombohedral modification of graphite. Greater difference comes from the fact that they considered a homogeneous single-crystal graphite/diamond transformation without any dangling bonds while we consider an interface that is, a heterogeneous structure, which requires the dangling bonds even when it is coherent. The experimental value can be even less if the mechanism of termination of the dangling bonds by sp^1 carbon atoms is essential.

In the same paper [7] the authors predicted disappearance of the need for thermal activation of the transition of rhombohedral graphite into diamond at (0 K, 80 GPa). This fact may be interpreted as attainment of the graphite spinodal point of the free energy, Eq. (25), see Fig. 2. Then, using Eqs. (2), (20), (22), and the data of [4], we obtain that $A_\xi(0\,\mathrm{K},80\,\mathrm{GPa})=6\Delta G_{G/D}(0\,\mathrm{K},80\,\mathrm{GPa})\approx 441.$ kJ/mol. Using a linear approximation for the pressure dependence of the coefficient A_ξ we can estimate $\partial A_\xi/\partial P\approx 1.79$ cm^3/mol. Notice that $\partial A_\xi/\partial P\approx V_G-V_D$.

The conclusion of [40] that high value of the diamond/graphite interfacial energy mostly is due to the significant number of dangling bonds on the interface allows us to estimate the slope of the temperature dependence of the barrier-height coefficient A_ξ. Indeed, any process that causes termination of the dangling bonds will decrease $\sigma_{D/G}$ and the coefficient A_ξ. Three mechanisms may be responsible for termination of the dangling bonds on the diamond/graphite interface: sp^1-hybridization, hydrogenization, and generation of 'free' electrons. In the present paper we will consider only the latter. The structure of the interface yields the number of the interface dangling bonds of about 5×10^{18} m^{-2}. Generation of 'free' electrons is a thermally activated process; at 4000 K the bulk concentration of 'free' electrons (1.5×10^{24} m^{-3}) will be sufficient to saturate all dangling bonds with the electrons. If we estimate the energy decrease from trapping an electron on the dangling bond to be ~ 1 eV, we arrive at the interface energy reduction of 0.8 J/m^2. Then, assuming that $l_{D/G}$ and the average molar volume do not change much with temperature, we can estimate from Eq. (27) the slope of the temperature dependence of the barrier-height coefficient to be $\partial A_\xi/\partial T\approx -0.05$ kJ/mol K. Thus the linear approximation of the barrier-height coefficient takes the form:

$$A_\xi(T,P)\left[\frac{\text{kJ}}{\text{mol}}\right] \approx 297.6 + 1.79 \times P[\text{GPa}] - 0.05 \times T[\text{K}] \quad (28)$$

Variation of A_ξ with temperature along the graphite/diamond phase-equilibrium boundary is shown in Fig. 5.

As one can see from Eq. (26) the interfacial energy of the carbon system is affected by the phase-transformation compression while the interfacial thickness is unaffected by the volume change. The effect of compression on the interfacial energy can be estimated as follows:

$$e \equiv \frac{\sigma_{D/G}(V_G \neq V_D)}{\sigma_{D/G}(V_G = V_D)} - 1 = \frac{V_G + V_D}{2(V_G - V_D)} \ln\frac{V_G}{V_D} - 1 \quad (29)$$

For the diamond/graphite transition this effect is relatively small, $e \approx 1.4\%$.

2.4. *Nucleation of diamond from liquid carbon*

Ghiringhelli et al. [14] conducted MD simulations of nucleation of diamond phase from liquid carbon using a semiempirical many-body potential that has been fit to the properties of solid and liquid carbon phases. The entire simulation box contained 2744 particles. The successful attempt at $T_A = 5000$ K and $P_A = 85$ GPa ('blue diamond' in Fig. 1) corresponded to the chemical potential difference (driving force) of $\Delta\mu_A = 0.60\, k_B T_A$. It resulted in the creation of a critical nucleus of $N_A = 110$ carbon atoms with the number density of $\rho_A = 191\,\text{nm}^{-3}$ and the total Gibbs free energy excess of $\Delta G_A = 25\, k_B T_A$. These numerical results were fitted into the Classical Nucleation Theory (CNT). Although the authors have to be complimented for their attempt to obtain the quantitative information regarding the nucleation process, one has to notice that matching their data to CNT was not justified because neither of the regular CNT assumptions – that a new-phase nucleus contains large number of atoms, the interface between the new and parent phase is infinitely thin, or that the interfacial energy is independent of the driving force – was satisfied in their case. For instance, we will show below that most of the volume of the critical nucleus was covered by the interfacial region.

The continuum theory provides a much better platform for comparison with the MD numerical simulations then CNT because neither of the CNT assumptions is used in the continuum theory. In Appendix, using the continuum theory, we derived the expressions for the total Gibbs free energy excess ΔG_{cn} and number of moles N_{cn} of the critical nucleus of a new phase in the infinite amount of the parent phase. These expressions were used to formulate a routine for the identification of the parameters of the continuum theory. Below this routine will be used for the parameters A_η and κ_η. For the free energy, Eq. (25), the terminal phases – diamond and liquid carbon – have the same structural OP $\xi = \xi_0$. Hence, the whole system of diamond nucleus in liquid carbon corresponds to $\xi = 0$ (the thick black horizontal line in Fig. 3). As the compression effect for diamond/graphite transition is rather small (see Eq. (29) and below) and $V_L - V_D \ll (V_L + V_D)/2$ at high temperature, we neglect this effect for the diamond/liquid-carbon system.

According to the routine developed in Appendix, one has to numerically resolve Eq. (A19) where the left-hand side is a particular function, $H(\eta_t)$, represented in Fig. A2 and the right-hand side is a number α obtained from experiments or simulations. Comparing the continuum-theory quantities

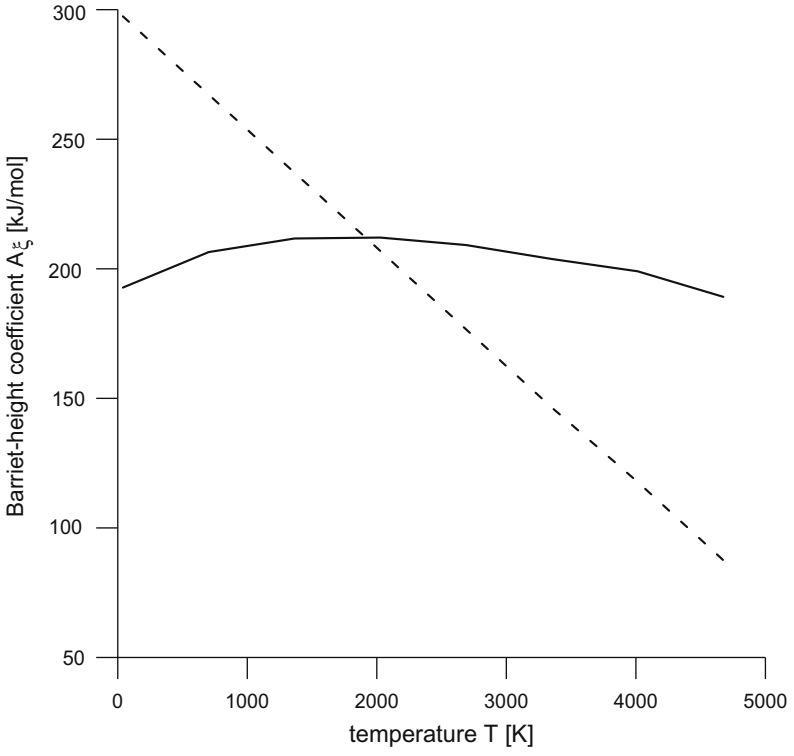

Fig. 5 – Barrier-height coefficient A_ξ (dashed line) and its critical value A^*_ξ (solid line) versus temperature along the graphite/diamond phase-equilibrium boundary.

with their numerical counterparts from Refs. [8,14] we find that $\Delta G_{cn} = \Delta G_A$, $\Delta G_{D/L} = \Delta\mu_A N_{Av}$, and $N_{cn} = N_A N_{Av}$ where N_{Av} is the Avogadro number. Hence:

$$\alpha \equiv \frac{\Delta G_{cn}}{N_{cn}\Delta G_{D/L}} = \frac{\Delta G_A}{N_A \Delta\mu_A} = -0.379$$
$$V_{cn} \equiv \frac{N_{cn}}{\bar{\rho}} = \frac{N_A}{\rho_A} = 0.576\ \mathrm{nm}^3 \quad (30)$$

Then, the numerical solution of Eq. (A19) yields (see Fig. A2):

$$\eta_t(\alpha) = 0.334. \quad (31)$$

Application of Eq. (A20) yields the values of the coefficients A_η and κ_η at ($T = 5000$ K, $P = 85$ GPa):

$$A_\eta = \frac{6|\Delta\mu_A|N_{Av}}{1-2\eta_t(\alpha)} = 374.\frac{\mathrm{kJ}}{\mathrm{mol}}$$
$$\kappa_\eta = A_\eta\left\{\frac{V_{cn}}{4\pi I_1[\eta_t(\alpha)]}\right\}^{2/3} = 2.46\times10^{-15}\frac{\mathrm{J\ m^2}}{\mathrm{mol}} \quad (32)$$

Using the values of A_η and κ_η we can estimate the diamond/liquid interface energy and thickness as following:

$$\sigma_{D/L} = \frac{\bar{\rho}}{6}\sqrt{\kappa_\eta A_\eta} = 1.603\frac{\mathrm{J}}{\mathrm{m}^2},$$
$$l_{D/L} = 4\sqrt{\frac{\kappa_\eta}{A_\eta}} = 0.324\ \mathrm{nm} \quad (33)$$

The present estimate of the diamond/liquid interfacial energy is in good but not perfect agreement with that of [14], 1.86 J/m^2, obtained through the comparison with CNT. We argue here that our estimate is more consistent. Indeed, given the volume of the critical nucleus in [14] of 0.576 nm^3 (see Eq. (30)) and assuming that it was a sphere, its radius would be 0.516 nm. Comparing this estimate with that of the interfacial thickness, Eq. (33), we can see that the thickness of the interface is more than a half of the radius of the critical nucleus. In Fig. 6 is depicted OP η versus the scaled distance from the center of the critical nucleus of diamond in liquid carbon. The graph also shows that the transition zone occupies a large portion of the critical nucleus. Thus, at least one assumption of CNT was not satisfied in the simulations of [14].

Also in Fig. 6 is depicted variation of the average coordination number C, defined by Eq. (17), along the radius of the critical nucleus of diamond in liquid carbon. Notice that the coordination number changes more abruptly from the diamond-like to liquid-like value in the transition zone than the OP. Another important feature to notice is that in the liquid phase the average coordination number falls below the value of 3, which on the microscopical level means presence of sp^1 hybridized atoms. Although this may be an artifact of the linear relationship, Eq. (17), it may also contain certain physical significance. Modeling of liquid and amorphous carbon shows that sp^1-carbon can be present in both materials, although not in high concentration. For instance, the fraction of sp^1-carbon in liquid carbon around the triple point can be as high as 15% although diamond and graphite remain essentially sp^1-carbon free. This means that sp^1-carbon plays an important role in transition states, mostly facilitating the continuity of the network and helping to eliminate the dangling bonds.

3. Applications of the theory

3.1. *Graphite/liquid-carbon interfacial energy*

A natural application of the developed model is to the problem of crystallization of graphite from liquid phase. Out of

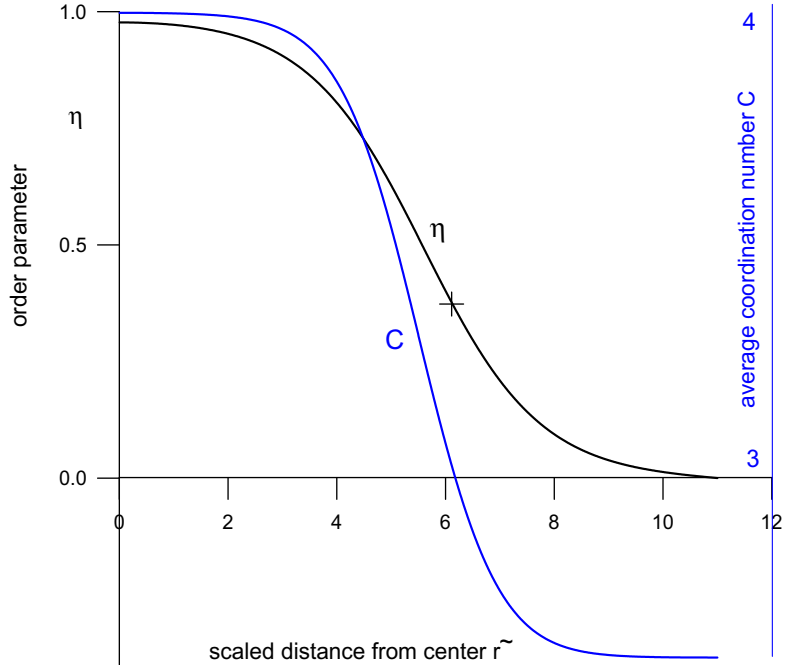

Fig. 6 – Order parameter η and average coordination number C versus the scaled distance from the center of the critical nucleus of diamond in liquid carbon at (T, P) that corresponds to the blue diamond point on the phase diagram of Fig. 1. (+)-transition state $\eta_t(\alpha)$.

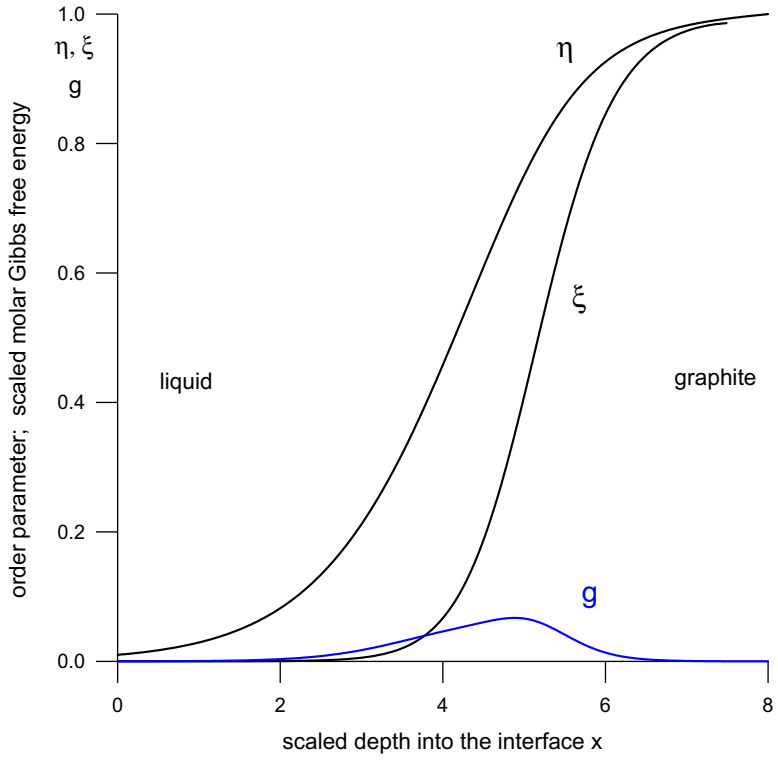

Fig. 7 – Spatial distribution of the crystallization OP, η, and structural OP, ξ, and scaled molar Gibbs free energy $g = (G - \mu)/A_\eta$ (blue line) for the graphite/liquid interface at (T, P) that corresponds to the 'black triangle' point on the phase diagram of Fig. 1. (For interpretation of the references to color in this figure legend, the reader is referred to the web version of this article.)

many aspect of graphite crystallization only the structure of the solid/liquid interface and the interfacial energy, $\sigma_{G/L}$, at the graphite melting line (the 'black triangle' point on the phase diagram in Fig. 1) will be considered here. The difference from the previously considered cases of diamond/liquid and diamond/graphite interfaces is that now both OP's, η and ξ, vary along the coordinate axis perpendicular to the plane of the interface. Hence, the 1D open-system equilibrium-state boundary-value problem for the graphite/liquid interface includes simultaneous equations, Eq. (11a), for both OP's. In addition to the driving forces of both processes – crystallization and structural – our model depends on the two sets of barrier-height and gradient-energy coefficients. These coefficients were identified in the previous section but at the temperatures and pressures different from those of the 'black triangle'. In the calculations below we used Eq. (28) for the coefficient A_ξ; all other coefficients were assumed to be temperature and pressure independent. The system of simultaneous equations was numerically solved and a separatrix that satisfies the boundary conditions, Eq. (11b) was found. In Fig. 3 is depicted the projection of the separatrix on the plane (η, ξ). In Fig. 7 are shown the spatial distributions of OP's and scaled molar Gibbs free energy, Eq. (25), along the coordinate axis perpendicular to the plane of the interface. Compare Figs. 3, 7 and notice that although the trajectory of the representative point of the interface crosses two critical lines, $\xi = \xi_t(\eta)$ and $\eta = \eta_t(\xi)$, Eq. (20), there is actually only one Gibbs free energy barrier on the path of this point.

Numerical calculations of the graphite/liquid interfacial energy, Eqs. (14) and (25), produced the value:

$$\sigma_{G/L} = 1.66 \frac{J}{m^2}. \tag{34}$$

Notice that this value is comparable to $\sigma_{D/L}$ and $\sigma_{G/D}$.

3.2. *Nanostructured amorphous carbon*

In Section 2.2 we discussed a possibility for a transition state to become thermodynamically stable in a closed system if the conditions of Eqs. (16) and (17) are fulfilled. In the present section we apply these conditions to the system described by Landau–Gibbs free energy, Eq. (25). Eq. (16) can be expressed as an inequality for the barrier-height coefficient:

$$A_\xi(T, P_E) < A^*_\xi \equiv 8(V_G - V_D)^2 \left| \left(\frac{\partial V}{\partial P}\right)_G + \left(\frac{\partial V}{\partial P}\right)_D \right|^{-1} \tag{35}$$

where its critical value, A^*_ξ, depends only on the equilibrium properties of the phases and is proportional to the transformation shrinkage squared[2]. In Fig. 5 the coefficient A_ξ, Eq. (28), and its critical value A^*_ξ are shown as functions of T along the graphite/diamond phase-equilibrium boundary. As one can see the condition of Eq. (35) is fulfilled for $T > 2000$ K.

[2] The critical value in Eq. (35) is 9/8 times greater if only the local stability of the transition state is required as opposed to the global one.

In Fig. 8 the graphite and diamond phases and the transition state are represented by their molar Helmholtz free energies as the functions of molar volume at 4000 K. One can see that there is a certain domain of molar volumes where the transition state has less Helmholtz free energy (more stable) than both bulk phases. Compare Fig. 8 with Fig. 2 and notice that the transition state has greater Gibbs free energy than both bulk phases for the same pressure. This means that although this state is not a stable phase under conditions of fixed pressure it can be stable under the conditions of fixed volume. However, the heterogeneous state that is, a mixture of graphite and diamond phases has lower Helmholtz free energy than any of the homogeneous ones in the domain between the equilibrium values of the molar volumes of the bulk phases (V_D, V_G). This means that in a closed system of the average molar volume from this domain a macroscopic (large enough) piece of carbon will break up into coexisting phases of diamond and graphite. The situation changes dramatically in nanostructures with the dimensions less than the critical size, Eq. (17): according to the analysis of [36] the transition state becomes globally stable (that is, with respect to all fluctuations of ξ) against the graphite and diamond phases and a mixture of the two.

Stabilization of the diamond/graphite transition state under the closed-system conditions allows us to conjecture that this state corresponds to the nanostructured amorphous carbon (na-C), which, as it was pointed out in the Section 1, is thermodynamically stable to a certain degree. Notice that formation of the stable na-C should be orientation dependent.

The above presented conjecture allows us to interpret results of the experiments on FIB irradiation of the surface of the single crystal CVD diamond film [18–20]. Ga^+-ion-beam scanning irradiation of the films produced nanodots and nanowires of the width approximately equal to the diameter of the beam that is ~ 20 nm [18–20]. The nanostructures were stable at the room temperature; their conductivity was smaller than that of the graphite but greater than that of the diamond. When annealed at approximately 1000 °C for 15–20 min the conductivity of the nanostructures always increased approaching that of the graphite phase. In the experiments of [18–20] the phase content of the nanostructures remained undetermined with the amorphous phase being a candidate. Irradiation of the film creates high temperature and pressure in the affected zone. However, there is no evidence that the irradiated material in these experiments was molten at any time and we assume that the entire transformation path passed in the solid state. Ga^+ ions most likely do not remain in the nanostructures because Ga does not form compounds with carbon. Then, according to the criterion, Eq. (35), at the temperature and pressure of irradiation the condition for the stabilization of the amorphous phase was met, see Fig. 5. The support for the amorphous structure of the produced states comes from the observed limited conductivity of the irradiated materials, which is due to the partial hybridization of the transition state, $0 < \xi_t < 1$. When the temperature decreases the amorphous phase becomes unstable but the slow kinetic processes do not allow the material to achieve the thermodynamic equilibrium state – the graphite

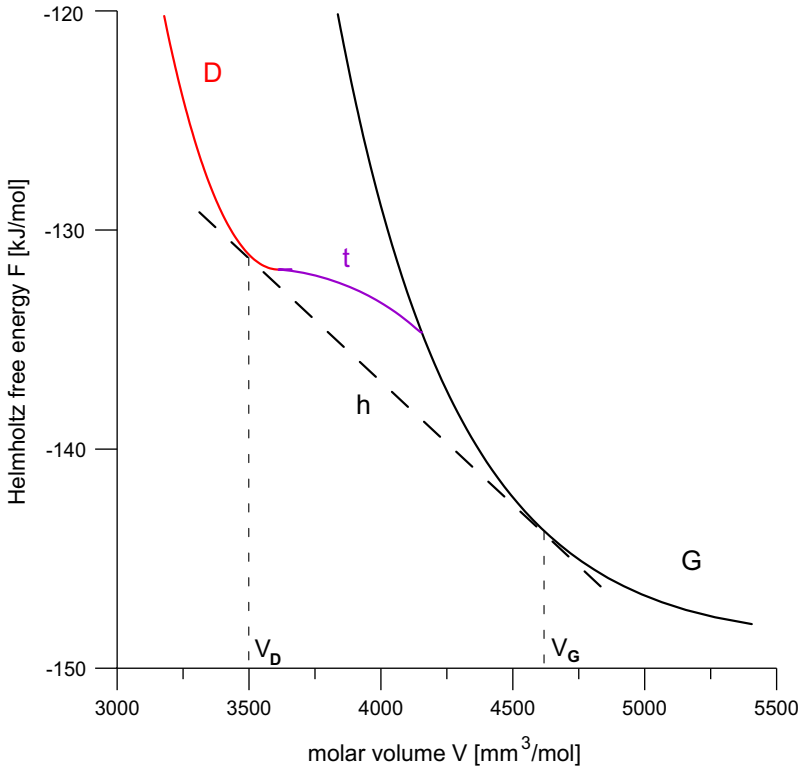

Fig. 8 – Helmholtz free energy *F* of the diamond (D) and graphite (G) phases, the transition (t) and heterogeneous (h) states as functions of the molar volume *V* at *T* = 4000 K using the calculations of [8] and Eq. (30).

phase. During annealing the kinetic processes speed up significantly which helps the system to restore thermodynamic equilibrium that is, transform the nanostructure into the stable graphite phase ($\xi_G = 0$).

The present theoretical study applies to a closed system of fixed volume, which is not completely the case for the surface irradiation experiments. To verify the theoretical predictions of the present research it would be very interesting to conduct an irradiation experiment where the transformation takes place completely under the surface of the film that is, in the bulk of a carbon film. This may be achieved by means of focused high energy ion irradiation [41,42], which is known to produce buried amorphous nanoclusters in diamond.

4. Discussion

In this paper we build a continuum theory of carbon phases, which ties up many seemingly unrelated data on carbon system. For the consistency of the theory it would be preferential to use the data from the same work or at least the works that use similar methods. Unfortunately such data are not available at present. That is why we used the data of a few different studies, which nevertheless we find quite consistent. The theory describes transformations between graphite, diamond and liquid carbon with the help of a Landau–Gibbs free energy which, in addition to temperature and pressure, depends on two order parameters: crystallization and structural. The thermodynamic data on the equilibrium (stable and metastable) phases were obtained from the database of [4] for low temperatures and the numerical study of carbon system in [8] for high temperatures. The Landau–Gibbs free energy contains two barrier-height and two gradient-energy coefficients, which were calculated from the data obtained in the studies of nucleation of diamond on graphite [40] and from liquid-carbon [14]. The results of [40] are applicable only to the specific, most favorable, diamond/graphite matching direction, which means that out of a few possible diamond/graphite barriers the value determined here is the lowest. On the microscopic level, in the transition zone the diamond crystal, which incorporates atoms with rigid sp^3 bonds, should match another carbon phase – liquid or graphite – composed of atoms with predominantly sp^2 bonds. As a result, there are certain similarities between the barrier heights of the two interfaces. Thus, similarity of the values of the diamond/graphite and diamond/liquid-carbon barrier-height coefficients, A_η and A_ξ, Eqs. (27) and (32), is due to similarities of the transition regions as opposed to the terminal phases because structurally graphite and liquid carbon are very different. The disparity of the values of the gradient-energy coefficients, κ_ξ and κ_η, Eqs. (27) and (32), with the latter being more than 4 times greater than the former can be explained by significantly greater level of stress in the diamond/graphite interface than in the diamond/liquid one. The boundary of the absolute stability of the graphitic phase, which was attained in the numerical calculations of the graphite–diamond transition in [7], we interpret here as the spinodal point of the Landau–Gibbs free energy. This result allowed us to calculate the pressure dependence of the coefficient A_ξ. The temperature dependence of this coefficient was estimated on the bases of the conclusion in [40] that high value of the diamond/graphite interfacial energy mostly is due to the significant number of dangling bonds on the interface. We have not found data in the literature that would allow us to estimate the temperature–pressure dependencies of other coefficients.

The continuum model yielded the value of $1.603\,J/m^2$ for the diamond/liquid-carbon interface energy as opposed to $1.86\,J/m^2$ obtained in [14] by comparing the MD simulation results with the Classical Nucleation Theory. We believe that our value is more consistent because it is not based on the comparison with CNT, which is not applicable here. The calibrated theory was also used for the analyses of the graphite/liquid-carbon interface energy, which can be used for numerical simulations of graphite crystallization and, to the best of our knowledge, has not been published yet. The obtained value of graphite/liquid-carbon interface energy, $1.66\,J/m^2$, is comparable to that of diamond/liquid-carbon and can also be explained by the similarities of the transition regions.

The diamond/liquid and graphite/liquid interfacial energies can be compared with the crystal/liquid interfacial energies of other elements of group IV of the periodic table. The values of the latter quantities acceptable for the comparison were obtained in numerical experiments using cleaving or capillary-fluctuation methods. They are (in J/m^2): $0.34 - 0.42$ for silicon (depending on the orientation of the interface) [43],[3] 0.165 for germanium, $0.055\,J/m^2$ for tin [45], and 0.057(4) for lead [46]. As one can see the interfacial energies of these materials depend strongly on the bond energies of the elements, with carbon being a strongly covalent material with the highest bond energy and tin and lead – a metal or semimetal with the least bond energy. A similar trend can be found in the surface energies (crystal/vapor) of C, Si and Ge where, however, the role of orientation and surface reconstruction is much more important [47].

We also analyzed stability of nanostructured amorphous carbon (na-C) and were able to interpret na-C as the transition state of the Landau–Gibbs free energy function. This conjecture helped us to explain results of the experiments on amorphization of carbon under conditions of FIB irradiation of CVD-diamond nanofilms [18–20]. Regardless of the theoretical interpretation, we think that the term 'amorphous carbon' is a misnomer. The problem with such nomenclature is that amorphization is usually associated with crystallization when amorphous state is understood as a failed crystal [48]. It should be distinguished from a phase or state that emerges as a result of an entirely solid-state transformation. For the lack of a better term such phases may be called *disordered solid phases*.

The present model may be extended to include other structural modifications of carbon. To include a carbine phase with predominantly sp^1 hybridization of carbon atoms the free energy $G(\eta, \xi)$ should have another minimum in the (η, ξ)-domain that corresponds to the average coordination

[3] Another value obtained experimentally, 0.68–0.69 at melting temperature and decreasing to about 0.32 for lower temperatures, is given in [44], but seems to be inconsistent here.

number $C \approx 2$. For the model to include other solid phases, e.g. BC-8 or hexagonal carbon, the free energy $G(\eta, \xi)$ should have additional minimum in the domain $\eta > 1$ or a third OP should be introduced.

Kinetics of the transformations is another direction of expansion of the present theory. It is possible to extract the kinetic coefficients from the numerical simulations of diamond nucleation rate in [14]. These data may be used for the large-scale modeling of graphite and diamond crystallization. The suggested framework may also be applied to an entirely different element of tremendous practical significance – silicon. These challenging problems will be dealt with in the later publications.

Acknowledgements

The authors would like to thank Drs. A. Zaitsev and L. Ghiringhelli for helpful discussion of the paper. This work was supported by ARO Grants 46499-MS-ISP, W911NF-06-1-0302 and 47145-00 01.

Appendix. 3D critical nucleus

Proper description of the process of nucleation is an important goal of the continuum theory of phase transitions. Thermodynamic data on the free energy excess and size of a critical nucleus can be successfully used for the identification of the parameters of the continuum method. The general strategy is the following: one obtains values of the free energy excess and volume of the critical nucleus of the new phase using other means of study, e.g. experiment or molecular simulations, and compares them with the similar values obtained by means of the continuum method. Cahn and Hilliard [49] (CH) considered this problem in the limit of a large driving force that is, the free energy difference between the parent and product phases. In the present Appendix the problem will be solved without the simplifying assumptions of the large driving force. The process of nucleation is affected by the difference of the densities of the parent and product phases. However, the compression effect of nucleation is not considered here. For the sake of brevity we will be considering nucleation for a solid phase from liquid, although the results are applicable to many different transformations.

The boundary-value problem for the crystallization OP variation can be obtained from Eq. (8) in the main text:

$$\kappa\nabla^2\eta = \frac{\partial G}{\partial \eta} \tag{A1}$$

$$|\nabla\eta| \to 0, \eta \to 0 \quad \text{for} \quad \mathbf{x} \to \infty \tag{A2}$$

$$\mu = G(T, P, \eta = 0) \equiv G_L(T, P) \tag{A3}$$

For a 3D spherically symmetric nucleus: $\nabla^2 = \frac{1}{r^2}\frac{d}{dr}\left(r^2\frac{d}{dr}\right)$ where r is the distance from the center of the nucleus. For the molar free energy of the system, Eqs. (4) and (25), r can be scaled as follows:

$$\tilde{r} = \frac{r}{\delta}; \quad \delta = \sqrt{\frac{\kappa}{A}} \tag{A4}$$

and the boundary-value problem, Eqs. (A1), (A2), (A3), takes the form:

$$\frac{d^2\eta}{d\tilde{r}^2} + \frac{2}{\tilde{r}}\frac{d\eta}{d\tilde{r}} + 2\eta(\eta - \eta_t)(1 - \eta) = 0, \tag{A5}$$

$$\frac{d\eta}{d\tilde{r}} = 0 \quad \text{at} \quad \tilde{r} = 0, \tag{A6}$$

$$\frac{d\eta}{d\tilde{r}} \to 0, \eta \to 0 \quad \text{at} \quad \tilde{r} \to \infty, \tag{A7}$$

that depends only on the transition state OP, Eqs. (20) and (22), as an external parameter:

$$\eta_t = \frac{1}{2} + 3\frac{\Delta G_{S/L}}{A} \tag{A8}$$

The solution of the boundary-value problem Eqs. (A5), (A6), (A7) is not a regular trajectory in the space $(\eta, d\eta/d\tilde{r})$ but a separatrix because there are three boundary conditions for a second-order ODE [29]. The problem Eqs. (A5), (A6), (A7) can be solved numerically by selecting a proper initial value $\eta_0 = \eta(\tilde{r} = 0)$ that allows the trajectory to satisfy other three boundary conditions.

The total free energy excess due to presence of the solid nucleus in a previously homogeneous liquid equals:

$$\Delta\mathcal{G}_{cn} = \mathcal{G}\{T, P, \mathcal{N}, \eta(\mathbf{r})\} - \mu\mathcal{N} \tag{A9}$$

Taking into account the expressions for the total free energy, Eqs. (4) and (5), and the mole number, Eq. (7), and assuming that densities of the phases are equal $\rho = \bar{\rho} = const(x)$, Eq. (A9) can be written as follows:

$$\Delta\mathcal{G}_{cn} = \bar{\rho}\int_{\mathcal{V}}\left[G(T, P, \eta) + \frac{1}{2}\kappa(\nabla\eta)^2 - \mu\right]d\mathbf{x} \tag{A10}$$

Using the Gaussian theorem together with the formula $\nabla(\eta\nabla\eta) = \eta\nabla^2\eta + (\nabla\eta)^2$, the equilibrium equation, Eq. (A1), and boundary condition, Eq. (A2), we obtain the relation:

$$\kappa\int_{\mathcal{V}}(\nabla\eta)^2 d\mathbf{x} = -\int_{\mathcal{V}}\eta\frac{\partial G}{\partial\eta}d\mathbf{x} \tag{A11}$$

Then using this relation and the boundary condition Eq. (A3) for Eq. (A10) we obtain the expression for the free energy of the 3D spherically symmetric $(d\mathbf{x} = 4\pi r^2 dr)$ critical nucleus of solid in liquid:

$$\Delta G_{cn} = 4\pi\bar{\rho}\delta^3\int_0^\infty\left[G(T, P, \eta) - G_L(T, P) - \frac{1}{2}\eta\frac{\partial G}{\partial\eta}\right]\tilde{r}^2 d\tilde{r} \tag{A12}$$

For the system with the molar free energy, Eq. (25), this expression takes the form:

$$\Delta\mathcal{G}_{cn} = 2\pi\bar{\rho}\delta^3 A\left[\frac{2}{3}(1 + \eta_t)I_3 - I_4\right] \tag{A13}$$

where we used the expressions for the n-th order moments of the OP distribution:

$$I_n(\eta_t) = \int_0^\infty \eta^n\tilde{r}^2 d\tilde{r} \tag{A14}$$

The number of moles in the nucleus is

$$N_{cn} = \int_{\mathcal{V}}\rho\eta d\mathbf{x}. \tag{A15}$$

For the 3D spherically symmetric nucleus this expression takes the form:

$$N_{cn} = 4\pi\bar{\rho}\delta^3 I_1 \tag{A16}$$

Thus, using Eqs. (A4), (8), (13), (16) we can formulate a routine for the identification of the coefficients A and κ:

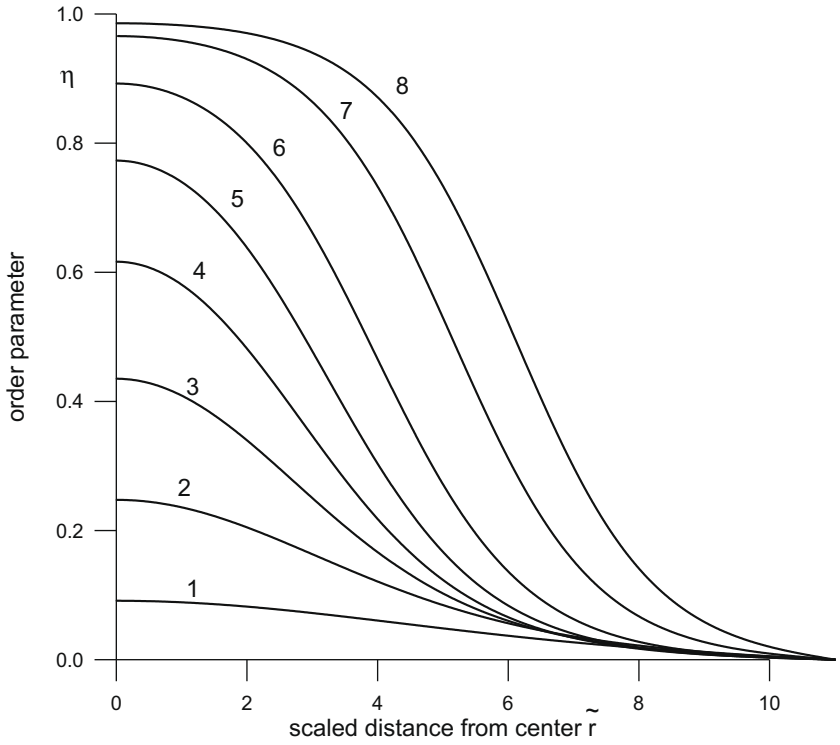

Fig. A1 – Solutions of the problem, Eqs. (A5), (A6), (A7) for different values of the transition state OP: (1) $\eta_t = 0.0041$; (2) 0.0558; (3) 0.1075; (4) 0.1592; (5) 0.2109; (6) 0.2625; (7) 0.3142; (8) 0.3401.

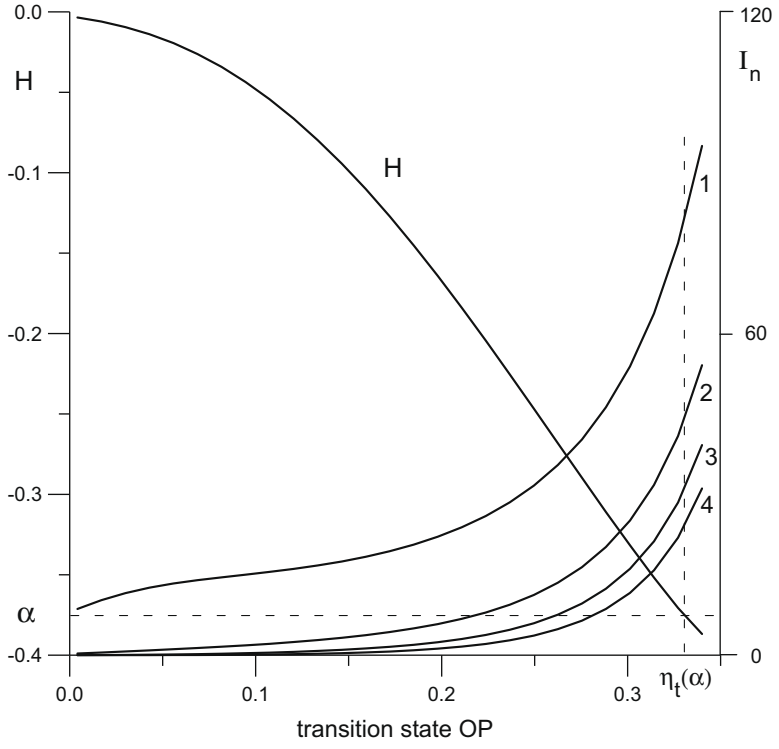

Fig. A2 – Function H, Eq. (A17), and the *n*th order moments I_n $(n = 1, 2, 3, 4)$, Eq. (A14), as the functions of the transition state OP η_t. The value of α is calculated in the main text.

1. Solve the boundary-value problem, Eqs. (A5)–(A7), for all appropriate values of η_t.
2. Compute the moments, Eq. (A14), using the solution from #1.
3. Compute the function:

$$H(\eta_t) \equiv \frac{(1+\eta_t)I_3(\eta_t) - 3/2I_4(\eta_t)}{(\eta_t - 1/2)I_1(\eta_t)} \tag{A17}$$

4. From the external data compute the following numbers:

$$\alpha \equiv \frac{\Delta\mathscr{G}_{cn}}{N_{cn}\Delta G_{S/L}}; \quad V_{cn} = \frac{N_{cn}}{\bar{\rho}} \tag{A18}$$

5. Find the value of the transition state OP η_t that satisfies the following equation:

$$H(\eta_t) = \alpha \tag{A19}$$

6. Find A and κ from the following relation:

$$A = \frac{3\Delta G_{S/L}}{\eta_t(\alpha) - 1/2}; \quad \kappa = A\left\{\frac{V_{cn}}{4\pi I_1[\eta_t(\alpha)]}\right\}^{2/3} \tag{A20}$$

7. If the value of the solid/liquid interfacial energy σ is independently available, verify the obtained values of A and κ by comparing the external value of σ to the continuum expression of the interfacial energy:

$$\sigma = \frac{\bar{\rho}}{6}\sqrt{\kappa A}. \tag{A21}$$

In Fig. A1 are plotted the solutions of the boundary-value problem, Eqs. (A5), (A6), (A7), which was numerically solved for the values of $0 < \eta_t < 0.4$. Notice that a recognizable interface exists only for $\eta_t \geqslant 0.16$ when the value of the OP at the center of the nucleus is greater than 0.5. In Fig. A2 are plotted function $H(\eta_t)$, Eq. (A17), and the moments I_n of orders $n = 1 - 4$, Eq. (A14). The rest of the routine, (##4–7), depends on the external data and is implemented in the main text.

The CH-routine suggested in [49] has an advantage over the present one (UA) in being able to avoid #5 after scaling out the transition state OP: $\eta \to \eta_t\eta$. The CH-routine assumes that $\eta \ll 1$. As one can see from Fig. A1 the CH-routine is valid for $\eta_t \leqslant 0.0041$. To estimate the accuracy of the CH-routine for the problem considered in the main text we computed η_t for a particular value of $\alpha = -0.379$ (see main text) using both methods: $\eta_{t,UA}(\alpha) = 0.334$; $\eta_{t,CH}(\alpha) = 0.227$. As one can see from Eq. (A20) and Fig. A2, different routines yield different values of the coefficients A and κ. Obviously, the source of the difference is the fact that the condition $\eta \ll 1$ is not satisfied for this value of α.

REFERENCES

[1] Bundy FP, Bassett WA, Weathers MS, Hemley RJ, Mao HK, Goncharov AF. The pressure–temperature phase and transformation diagram for carbon; updated through 1994. Carbon 1996;34:141–53.

[2] Togaya M. Pressure dependence of the melting temperature of graphite and the electrical resistivity of liquid carbon. Phys Rev Lett 1997;79:2474–7.

[3] Brygoo S, Henry E, Loubeyre P, Eggert J, Koenig M, Loupias B, et al. Laser-shock compression of diamond and evidence of a negative-slope melting curve. Nat Mater 2007;6:274–7.

[4] Fried LE, Howard WM. Explicit Gibbs free energy equation of state applied to the carbon phase diagram. Phys Rev B 2000;61:8734–43.

[5] Mailhiot C, McMahan AK. Atmospheric-pressure stability of energetic phases of carbon. Phys Rev B 1991;44:11578–91.

[6] Correa AA, Bonev SA, Galli G. Carbon under extreme conditions: phase boundaries and electronic properties from first-principles theory. PNAS 2006;103:1204–8.

[7] Fahy S, Louie SG, Cohen ML. Pseudopotential total energy study of the transition from rhombohedral graphite to diamond. Phys Rev B 1986;34:1191–9.

[8] Ghiringhelli LM, Los JH, Meijer EJ, Fasolino A, Frenkel D. Modeling the phase diagram of carbon. Phys Rev Lett 2005;94:145701–4.

[9] van Thiel M, Ree FH. Theoretical description of graphite, diamond, and liquid phases of carbon. Inter J Thermphys 1989;10:227–36.

[10] Glosli J, Ree FH. Liquid–liquid phase transition in carbon. Phys Rev Lett 1999;82:4659–62.

[11] Wu CJ, Glosli JN, Galli G, Ree FH. Liquid–liquid phase transition in elemental carbon: a first-principles investigation. Phys Rev Lett 2002;89:135701–4.

[12] Wang X, Scandolo S, Car R. Carbon phase diagram from *ab initio* molecular dynamics. Phys Rev Lett 2005;95:185701–4.

[13] Fyta MG, Remediakis IN, Kelires PC. Energetics and stability of nanostructured amorphous carbon. Phys Rev B 2003;67:035423–6.

[14] Ghiringhelli LM, Valeriani C, Meijer EJ, Frenkel D. Local structure of liquid carbon controls diamond nucleation. Phys Rev Lett 2007;99:055702–4.

[15] Korsunskaya IA, Kamenetskaya DS, Aptekar IL. Fiz Metal Metalloved 1972;34:942 (Russian); English version in: Phys Met Metallogr (USSR) 1972;34:39.

[16] Ferrari AC, Libassi A, Tanner BK, Stolojan V, Yuan J, Brown LM, et al. Density, sp3 fraction, and cross-sectional structure of amorphous carbon films determined by X-ray reflectivity and electron energy-loss spectroscopy. Phys Rev B 2000;62:11089–103.

[17] Casiraghi C, Robertson J, Ferrari AC. Diamond-like carbon for data and beer storage. Mater Today 2007;10:44–53.

[18] Zaitsev AM. Carbon nanowires made on diamond surfaces by focused ion beam. Phys Stat Solidi (a) 2005;202:R116–8.

[19] Zaitsev AM, Dobrinets IA. Carbon nanodots made on diamond surfaces by focused ion beam. Phys Stat Solidi (a) 2006;203:R35–7.

[20] Zaitsev AM, Levine AM, Zaidi SH. Temperature and chemical sensors based on FIB-written carbon nanowires. IEEE Sensors J 2008;8:849–56.

[21] Efstathiadis H, Akkerman Z, Smith FW. Atomic bonding in amorphous carbon alloys: a thermodynamic approach. J Appl Phys 1996;79:2954–67.

[22] Akkerman Z, Efstathiadis H, Smith FW. Thermal stability of diamond-like carbon films. J Appl Phys 1996;80:3068–75.

[23] Marks NA. Thin film deposition of tetrahedral amorphous carbon: a molecular dynamics study. Diamond Relt Mater 2005;14:1223–31.

[24] Liu H, Dandy DS. Studies on nucleation process in diamond CVD: an overview of recent developments. Diamond Relt Mater 1995;4:1173–88.

[25] Landau LD. On the theory of phase transitions. Phys Zs Sowjet 1937;11:26–42. see also: Collected Papers of L.D. Landau, Ter-Haar D editor; London: Gordon and Breach; 1967. p. 193–209.

[26] Landau LD, Lifshitz EM. Statistical physics. 3rd ed. Oxford: Pergamon Press; 1980. p. 471–2.

[27] Echebarria B, Folch R, Karma A, Plapp M. Quantitative phase-field model of alloy solidification. Phys Rev E 2004;70:061604–22.

[28] Umantsev A. Identification of material parameters for continuum modeling of phase transformations in multicomponent systems. Phys Rev B 2007;75:024202–9.
[29] Poston T, Stewart I. Catastrophe theory and its applications. London: Pitman; 1978.
[30] Landau LD. X-ray scattering of crystals in the neighborhood of the Curie point. Phys Zs Sowjet 1937;12:123–32. see also: Collected Papers of L.D. Landau, Ter-Haar D editor; London: Gordon and Breach; 1967. p. 233–42.
[31] Ginzburg VL, Landau LD. On the theory of superconductivity. Sov Phys JETP 1951;20:1064.
[32] Cahn JW, Hilliard JE. Free energy of a nonuniform system. I. Interfacial energy. J Chem Phys 1958;28:258–67.
[33] Gelfand IM, Fomin SV. Calculus of variation. New York: Prentice-Hall; 1963.
[34] Gibbs JW. The scientific papers, vol. 1. New York: Dover; 1961. p. 229–30.
[35] Umantsev A. Continuum theory of interfacial segregation. Phys Rev B 2001;64:075410–9.
[36] Umantsev A. Thermodynamic stability of amorphous phases in pure substances. J Stat Phys. doi:10.1007/s10955.009.9765.6.
[37] Ramakrishnan TV, Yussouff M. First-principles order-parameter theory of freezing. Phys Rev B 1979;19:2774–5.
[38] Dmitriev VP, Rochal SB, Gufan YuM, Toledano P. Reconstructive transitions between ordered phases: the martensitic fcc-hcp and the graphite–diamond transitions. Phys Rev Lett 1989;62:2495–8.
[39] Toledano P, Dmitriev VP. Reconstructive phase transitions. Singapore: World Scientific; 1996. p. 292–9.
[40] Lambrecht WRL, Lee CH, Segall B, Angus JC, Li Z, Sunkara M. Diamond nucleation by hydrogenation of the edges of graphite precursors. Nature 1993;364(6433):607–10.
[41] Stephan A, Meijer J, Weidenmüller U, Röcken H, Bukow HH, Burchard M, et al. The heavy ion micro-projection setup at Bochum. Nucle Instrum Meth Phys Res Sect B: Beam Interact Mater Atoms 2001;181(1–4 July):39–43.
[42] Zaitsev AM. High energy ion implantation into diamond and cubic boron nitride. Nucle Instrum Meth Phys Res Sect B: Beam Interact Mater Atoms 1991;62(1 November): 81–98.
[43] Apte PA, Zeng XC. Anisotropy of crystal-melt interfacial free energy of silicon by simulation. Appl Phys Lett 2008;92:221903–4.
[44] Jian Z, Kuribayashi K, Jie W, Chang F. Solid–liquid interface energy of silicon. Acta Materialia 2006;54:3227–32.
[45] Ravelo RJ, Baskes MI. Free energy calculations of the Cu–Sn interfaces. Mater Res Soc Symp Proc 1996;398:287–93.
[46] Hoyt JJ, Asta M, Karma A. Atomistic and continuum modeling of dendritic solidification. Mater Sci Eng 2003;R41: 121–63.
[47] Stekolnikov AA, Furthmuller J, Beschtedt F. Absolute surface energies of group-IV semiconductors: dependence on orientation and reconstruction. Phys Rev B 2002;65: 115310–8.
[48] Zallen R. The physics of amorphous solids. Weinheim, Germany: Wiley; 2004.
[49] Cahn JW, Hilliard JE. Free energy of a nonuniform system. III. Nucleation in a two-component incompressible fluid. J Chem Phys 1959;31:688–99.